

Article

Improvement Effect of Ni to Pd-Ni/SBA-15 Catalyst for Selective Hydrogenation of Cinnamaldehyde to Hydrocinnamaldehyde

Shiying Han, Yunfei Liu, Jiang Li, Rui Li, Fulong Yuan * and Yujun Zhu * 

Key Laboratory of Functional Inorganic Material Chemistry, Ministry of Education, School of Chemistry and Materials, Heilongjiang University, Harbin 150080, China; hsyhljdx@163.com (S.H.); 18724639744@163.com (Y.L.); lijian895243@163.com (J.L.); liruihljdx@163.com (R.L.)

* Correspondence: yuanfulong@hlju.edu.cn (F.Y.); yujunzhu@hlju.edu.cn (Y.Z.); Tel.: +86-451-8660-9650 (Y.Z.)

Received: 12 March 2018; Accepted: 27 April 2018; Published: 11 May 2018



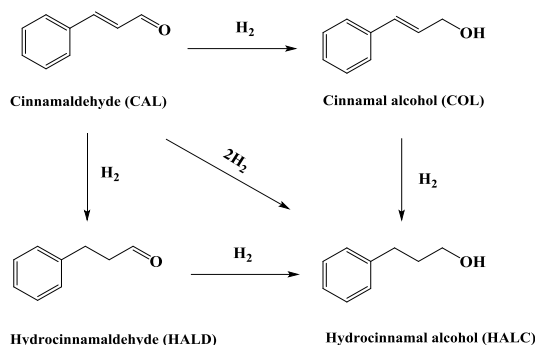
Abstract: A series of Pd-Ni bimetallic catalysts supported on SBA-15 (0.2%Pd-x%Ni/SBA-15, $x = 0.4, 0.7,$ and 1.2) were prepared through the impregnation method combined with the NaBH_4 reduction method. X-ray diffraction (XRD), N_2 adsorption-desorption, X-ray photoemission spectroscopy (XPS) and transmission electron microscope (TEM) were used to characterize the prepared catalysts. All the synthesized catalysts were evaluated for the liquid-phase hydrogenation of cinnamaldehyde (CAL). The addition of Ni obviously enhanced the CAL conversion and selectivity of C=C hydrogenation to hydrocinnamaldehyde (HALD) over the 0.2%Pd-x%Ni/SBA-15 catalysts. Meanwhile, 0.2%Pd-1.2%Ni/SBA-15 showed the best performance with 96.3% conversion and 87.8% selectivity toward HALD. This improvement was attributed to the synergistic effect between the Pd and Ni nanoparticles, enhancing the dispersion of Pd metal particles and increasing the content of surface Pd^0 species. In addition, the influences of a few reaction factors including H_2 pressure, reaction temperature, and reaction time were studied over 0.2%Pd-1.2%Ni/SBA-15.

Keywords: selective hydrogenation; cinnamaldehyde; hydrocinnamaldehyde; synergistic effect; Pd-Ni/SBA-15

1. Introduction

The selective catalytic hydrogenation of α, β -unsaturated carbonyl compounds to unsaturated alcohols or saturated aldehydes is an important step for the production of a great deal of chemicals, for instance, pharmaceuticals, spices, and fragrances [1–3]. Cinnamaldehyde (CAL) is a typical α, β -unsaturated aldehyde, which can produce various product distributions through its hydrogenation route (Scheme 1). Recently, hydrocinnamaldehyde (HALD), obtained by C=C hydrogenation, was considered as a vital intermediate in the process of synthesizing pharmaceuticals, which could be applied in HIV treatment [4,5]. Although the reduction of the C=C group is favorable thermodynamically relative to the activation of the C=O group, developing high-performance catalysts to improve the selectivity of C=C hydrogenation is still a great challenge.

Actually, a large number of catalytic systems have been used to study the hydrogenation of CAL. We also have investigated in detail the CAL hydrogenation by using all sorts of catalysts consisting of Pt/Graphene [6], Pt/CNS and Pd/CNS [7], Pt-Mo₂N/SBA-15 [8], Pd-WN/SBA-15 [9], and Co-Pt/SBA-15 [10]. In general, Pt [11–13], Ru [14,15], Au [16], Ir [17,18], Co [19,20], Cu [21,22] are conducive to the C=O bond hydrogenation to generate cinnamal alcohol (COL), while Pd [23,24], Rh [25,26], Ni [27–29] prefer a higher selectivity to the C=C bond, thus leading to the production of HALD.



Scheme 1. Reaction routes for the hydrogenation of cinnamaldehyde (CAL).

Recently, many reported studies have used bimetallic catalysts to investigate CAL selective hydrogenation. For example, Yang et al. [30] prepared a series of PdAu supported on mesoporous silica catalysts, which showed that PdAu/MSN catalysts significantly improved activity four times higher than the Pd/MSN catalyst. Zheng et al. [31] intensively discussed the hydrogenation of CAL over Co-Pt as well as Cu-Pt bimetallic catalysts supported on SiO₂, and compared the activity with Co, Cu, and Pt monometallic catalysts. The results suggested that bimetallic catalysts including Co-Pt and Cu-Pt showed greatly higher activity when compared with the monometallic part. In addition, the bimetallic Co-Pt catalyst favored the selectivity of C=O hydrogenation, whereas the bimetallic Cu-Pt catalyst promoted the hydrogenation of the C=C bond. Sun et al. [32] investigated the strong interaction between Au and Pt nanoparticles for the hydrogenation of CAL; Pt_m[^]Au immobilized on SiO₂ support showed higher activity and selectivity than monometallic Pt/SiO₂ and Au/SiO₂ catalysts. Lin et al. [5] pointed out that the deposition of a tiny amount of Ir to Ni/TiO₂ could evidently improve the performance of CAL hydrogenation where the intensive interaction between Ni and Ir changed the chemical state of surface Ni species, resulting in obvious enhanced activity when compared with the monometallic Ni/TiO₂ catalyst. Obviously, bimetallic catalysts can greatly improve the activity of CAL hydrogenation and the selectivity to desired products. In general, the selective hydrogenation of the C=C bond of CAL over different heterogeneous catalysts are summarized in Table S1.

In order to obtain metal-based catalysts with superior performance, the best method is to prepare evenly dispersed metal nanoparticles on a large specific surface area support, for instance, mesoporous carbon, silica, alumina, and so on [24,33–35]. Particularly, ordered mesoporous siliceous material SBA-15 is widely used as the support candidate due to its suitable pore size and large pore volume as well as high specific surface area [36,37]. In our previous work, we prepared a series of Pt-Co bimetallic catalysts supported on SBA-15 with various Pt/Co ratios where the synthesized Pt-Co/SBA-15 catalysts exhibited a marked enhancement in activity when compared with Pt/SBA-15, which was attributed to the generation of the Pt-Co alloy to increase the amount of surface Pt⁰ species [10]. In addition, the Pd-WN/SBA-15 samples were synthesized, and the results indicated that the addition of WN could lead to greatly enhanced performance and good reusability for the ternary Pd-WN/SBA-15 catalyst. This improvement was assigned to the strong interaction of Pd and WN leading to an increase in the ratio of surface Pd⁰ species as well as a decrease in the Pd particle size on the SBA-15 supported Pd-WN catalyst [9].

Based on the above descriptions, we successfully synthesized a variety of PdNi bimetallic catalysts supported on SBA-15 (0.2%Pd-x%Ni/SBA-15, x = 0.4, 0.7, and 1.2), and the influences of Ni content on the selective hydrogenation of CAL over bimetallic catalysts were investigated. The results showed that synthesized bimetallic 0.2%Pd-x%Ni/SBA-15 catalysts exhibited superior performance in the hydrogenation of CAL to HALD than their monometallic counterparts. It was discovered that the addition of Ni could enhance the dispersion of Pd nanoparticles and increase the amount of surface Pd⁰ species, resulting from the strong interaction between Pd and Ni nanoparticles. The study provides a strategy for enhancing conversion and selectivity with a much lower usage of Pd.

2. Results and Discussion

X-ray fluorescence spectrometry (XRF) analysis was carried out to measure the actual Pd and Ni contents for all samples. The theoretical Pd loading amount was 0.5 wt % for all catalysts, and the theoretical Ni loading amount was 0.5 wt %, 1.0 wt %, and 1.5 wt %, respectively. According to the XRF analysis, the measured Pd loading amount was about 0.2 wt % for all catalysts, whereas the loading amount of Ni increased along with the theoretical value, which was 0.40 wt %, 0.69 wt %, and 1.24 wt %, respectively. In order to make the experimental description more accurate, the catalysts were named using the actual loading amount of Pd and Ni. As the actual loading amount of Pd for all catalysts was similar to 0.2%, the Pd amount was denoted as 0.2% for convenience. Therefore, the catalysts were denoted as 0.2%Pd- x %Ni/SBA-15 ($x = 0.4, 0.7, \text{ and } 1.2$).

2.1. Texture Structure Measurement

Figure 1 displays the low-angle X-ray diffraction (XRD) patterns for 0.2%Pd/SBA-15 (b) catalyst and 0.2%Pd- x %Ni/SBA-15 (c–e) samples. All samples and the SBA-15 support exhibited typical (100), (110), (200) diffractions at 2θ of $0.5\text{--}2^\circ$, which was associated with the highly ordered hexagonal space group p6 structure of the SBA-15 host [38,39]. In addition, the result showed that the highly ordered hexagonal mesoporous structure of SBA-15 remained unchanged with the impregnation of Pd and Ni particles. Compared with the SBA-15 (a) support, the (100) reflection peak for all samples shifted to a high-angle direction, which demonstrated that Pd and Ni were scattered into the SBA-15 mesoporous channels. In addition, it was obvious that the 0.2%Pd/SBA-15 (b) and 0.2%Pd- x %Ni/SBA-15 (c–e) samples showed a much lower intensity of the (100) reflection peak relative to the SBA-15 support, suggesting the decrease of the mesoporous ordering of SBA-15.

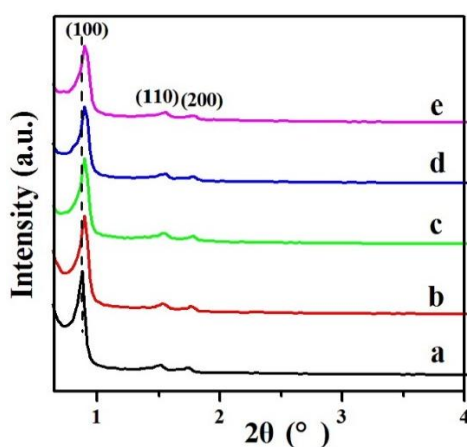


Figure 1. Low-angle XRD patterns of (a) SBA-15, (b) 0.2%Pd/SBA-15, (c) 0.2%Pd-0.4%Ni/SBA-15, (d) 0.2%Pd-0.7%Ni/SBA-15, (e) 0.2%Pd-1.2%Ni/SBA-15.

The mesoporous structure of the samples was also studied by nitrogen adsorption-desorption. As displayed in Figure 2, the isotherms of the 0.2%Pd/SBA-15 (b) and 0.2%Pd- x %Ni/SBA-15 (c–e) samples exhibited a representative IV isotherm with an obvious hysteresis loop in the range of P/P_0 of 0.6–0.8. The supported catalysts displayed cylindrical channels with a narrow pore size distribution and were similar to the parent SBA-15 (a), which was inconsistent with the result of low-angle XRD.

At the same time, the porosity parameters are presented in Table 1. The specific surface area of the 0.2%Pd/SBA-15 sample decreased to $635 \text{ m}^2/\text{g}$ from $745 \text{ m}^2/\text{g}$ of SBA-15, with the pore volume of 0.2%Pd/SBA-15 decreasing to $1.04 \text{ cm}^3/\text{g}$ from $1.06 \text{ cm}^3/\text{g}$ of SBA-15, which can be attributed to the introduction of Pd nanoparticles occupying the mesopore channels of SBA-15, resulting in the reduction of the mesopore width. Importantly, after the addition of Ni, the corresponding physicochemical properties further decreased. The Brunauer-Emmett-Teller (BET) specific surface

area and pore volume of 0.2%Pd-0.4%Ni/SBA-15 decreased to 627 m²/g and 1.03 cm³/g, respectively. For 0.2%Pd-0.7%Ni/SBA-15, the surface area as well as pore volume decreased to 595 m²/g and 0.97 cm³/g, respectively. The corresponding data for 0.2%Pd-1.2%Ni/SBA-15 were further reduced to 578 m²/g and 0.96 cm³/g. The significant decreases for the 0.2%Pd-x%Ni/SBA-15 samples in these physicochemical parameters suggested that the addition of Ni to the 0.2%Pd/SBA-15 sample further occupied the surface and pore of the support. Moreover, the highly ordered mesoporous channel remained constant with the impregnation of Pd and Ni, demonstrating that Pd and Ni might be evenly dispersed on the mesopores of the SBA-15 support. Besides, the pore size of all samples uniformly lay at about 6.0 nm (Figure S1), slightly lower when compared with the pores of the SBA-15 support, suggesting that the pore size of the support was occupied mildly by the introduction Pd and Ni.

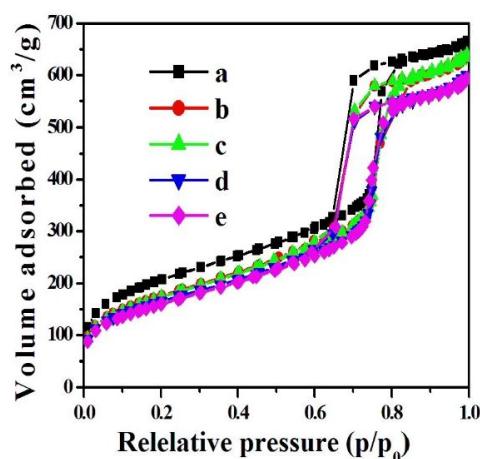


Figure 2. Nitrogen adsorption-desorption isotherms for (a) SBA-15, (b) 0.2%Pd/SBA-15, (c) 0.2%Pd-0.4%Ni/SBA-15, (d) 0.2%Pd-0.7%Ni/SBA-15, (e) 0.2%Pd-1.2%Ni/SBA-15.

Table 1. Relevant physicochemical properties of the different samples.

Sample	Metal Content ^a (wt %)		S _{BET} ^b (m ² /g)	V _{pore} ^b (cm ³ /g)	Pore Size ^b (nm)
	Pd	Ni			
SBA-15	-	-	745	1.06	6.1
0.2%Pd/SBA-15	0.16	-	635	1.04	6.0
0.2%Pd-0.4%Ni/SBA-15	0.18	0.40	627	1.03	6.0
0.2%Pd-0.7%Ni/SBA-15	0.18	0.69	595	0.97	6.0
0.2%Pd-1.2%Ni/SBA-15	0.19	1.24	578	0.96	6.0
0.2%Pd-1.2%Ni/SBA-15-used ^c	0.17	1.20	597	1.01	6.1

^a The loading content of Pd and Ni determined by XRF; ^b Derived from N₂ adsorption-desorption isotherms;

^c 0.2%Pd-1.2%Ni/SBA-15 sample after two catalytic runs.

The wide-angle XRD patterns for the 0.2%Pd/SBA-15 (b) and 0.2%Pd-x%Ni/SBA-15 (c–e) samples are displayed in Figure 3. As shown in the figure, all samples presented a broad peak of SiO₂ at approximately 22.5°. In addition, there were not the diffraction peaks of Pd and Ni, meaning that the Pd and Ni nanoparticles were highly dispersed on the support, which is consistent with previous reports [40,41]. After increasing the Pd loading amount to 0.9%Pd/SBA-15, the XRD pattern of the samples displayed a characteristic peak at 39.2° (Figure S2), matching the Pd (111) plane with a face-centered cubic (fcc) structure, whereas the peak belonging to Ni was invisible for all samples. In addition, the reflection peak of Pd (111) clearly shifted to a high angle direction and its intensity gradually reduced along with the increase in Ni loading amount. Moreover, the reflection peak of Pd (111) could not be observed for 0.9%Pd-1.2%Ni/SBA-15, indicating that the modification of Ni could improve the dispersion of Pd nanoparticles on the SBA-15 support and achieve a much smaller Pd

particle size. This could be illustrated by the strong interaction of Pd and Ni and that the addition of Ni can inhibit the growth of Pd nanoparticles.

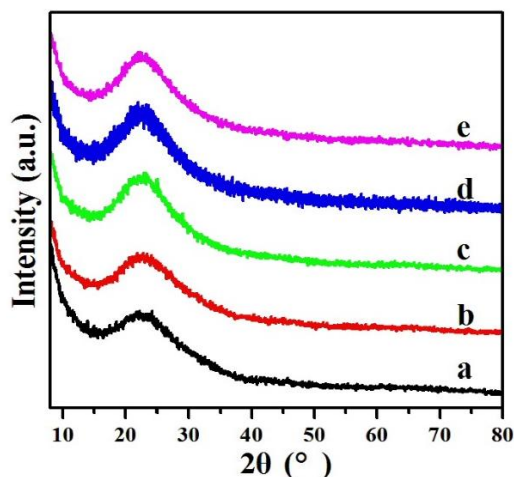


Figure 3. Wide-angle XRD patterns of (a) SBA-15, (b) 0.2%Pd/SBA-15, (c) 0.2%Pd-0.4%Ni/SBA-15, (d) 0.2%Pd-0.7%Ni/SBA-15, (e) 0.2%Pd-1.2%Ni/SBA-15.

2.2. TEM Analysis

The transmission electron microscope (TEM) analysis was used to characterize the structure of the synthesized catalysts as well as to provide effective proof of the distribution of nanoparticles (Figure 4). As a first observation, all samples exhibited the typical ordered structure of mesoporous SBA-15, which were in consistent with the results of the low-angle XRD and N_2 adsorption-desorption isotherms measurements. Figure 4a–d present the TEM micrographs of different areas acquired for the 0.2%Pd/SBA-15 (a–b) and 0.2%Pd-1.2%Ni/SBA-15 (c–d) samples. It was noteworthy that no Pd and Ni particles were detected in the TEM images. According to the XRF test, there was only a small amount of metals loading on the SBA-15 support. The loading amount of metals was so low that much smaller nanoparticles (less than 1 nm) could be formed in the 0.2%Pd-x%Ni/SBA-15 samples. Thus, the highly dispersed metal particles were not clearly observed.

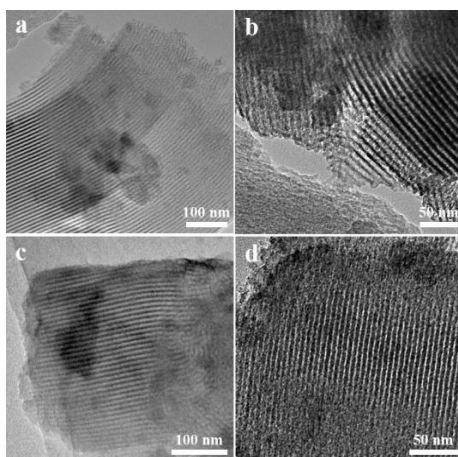


Figure 4. TEM images of (a,b) 0.2%Pd/SBA-15; (c,d) 0.2%Pd-1.2%Ni/SBA-15.

In order to prove the role of Ni, the TEM images of the 0.9%Pd/SBA-15 and 0.9%Pd-1.2%Ni/SBA-15 catalysts with high Pd content were also measured (Figure S3). Obviously, nanoparticles with an uneven distribution could be observed for 0.9%Pd/SBA-15. The lattice spacing

in the HR-TEM image (Figure S3b) was 0.223 nm, which was recognized as the (111) plane of Pd. However, after the introduction of Ni, the nanoparticles were highly distributed on the pore channel of the SBA-15 support and no large aggregated particles were observed. In addition, no observable crystal plane of Pd could be found for the 0.9%Pd-1.2%Ni/SBA-15 sample, indicating that the introduction of Ni can control the crystallization of Pd. This finding agrees well with the result of the wide-angle XRD analysis, which also pointed out that the impregnation of Ni could improve the dispersion of Pd particles on the SBA-15 support.

2.3. XPS Analysis

In order to examine the surface properties and the electronic states of Pd, the X-ray photoemission spectroscopy (XPS) analysis was conducted for the 0.2%Pd/SBA-15 and 0.2%Pd-*x*%Ni/SBA-15 catalysts. As illustrated in Figure 5A, the XPS in the range of 333–345 eV was ascribed to the Pd3d region. The Pd3d_{5/2} and Pd3d_{3/2} peaks at higher binding energies (337.6 and 342.7 eV) were described to the Pd²⁺ species and the Pd3d_{5/2} and Pd3d_{3/2} peaks at lower binding energies (335.0 and 340.6 eV) were attributed to the Pd⁰ (metallic palladium) [30,42]. However, there was a shift of 0.1–0.5 eV towards high binding energy for three 0.2%Pd-*x*%Ni/SBA-15 (b–d) bimetallic catalysts with respect to the 0.2%Pd/SBA-15 (a) catalyst, which can be ascribed to the reduction in the particle size of Pd with the addition of Ni [43–45]. The above result further proved that the introduction of Ni could better disperse the Pd nanoparticles and was in line with the results of the wide-angle XRD and TEM analysis.

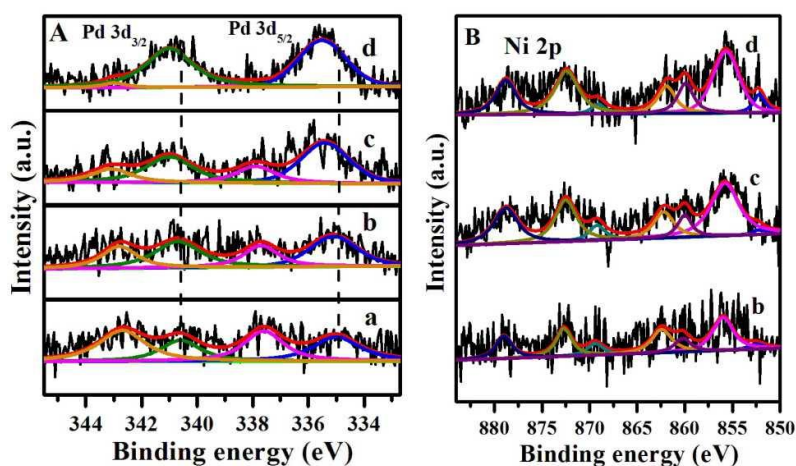
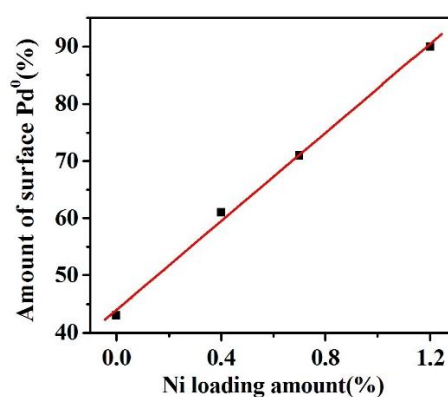


Figure 5. XPS spectra of (A) Pd3d and (B) Ni2p of the catalysts (a) 0.2%/SBA-15, (b) 0.2%Pd-0.4%Ni/SBA-15, (c) 0.2%Pd-0.7%Ni/SBA-15, (d) 0.2%Pd-1.2%Ni /SBA-15.

In addition, the shift to the high binding energy of Pd also suggested that the surface charge density of Pd particles increased with the amount of Ni. In order to quantify the surface Pd species, the contents of the surface Pd⁰ and Pd²⁺ species were calculated by the relative peak area listed in Table 2. The fractions of the Pd⁰ and Pd²⁺ species in 0.2%Pd/SBA-15 were approximately 43% and 57%, respectively. It is notable that the content of metallic Pd⁰ increased from 61% to 90% upon increasing the Ni loading amount from 0.4 wt % to 1.2 wt %, which revealed an electron transfer from Ni to Pd, consequently leading to the increase in the surface Pd⁰ species. Interestingly, a good linear relationship of the amount of surface Pd⁰ against the Ni loading amount was found on the 0.2%Pd-*x*%Ni/SBA-15 catalysts presented in Figure 6. The above results confirmed that the presence of Ni could significantly improve the formation of surface Pd⁰, which is in keeping with the results from the reported literature [46].

Table 2. XPS data of the Pd3d levels for different samples.

Sample	Pd Species	Pd Species BE (eV)		Content of Pd Species (%)
		3d _{5/2}	3d _{3/2}	
0.2%Pd/SBA-15	Pd ⁰	335.0	340.6	43
	Pd ²⁺	337.6	342.7	57
0.2%Pd-0.4%Ni/SBA-15	Pd ⁰	335.1	340.7	61
	Pd ²⁺	337.7	342.9	39
0.2%Pd-0.7%Ni/SBA-15	Pd ⁰	335.4	341.0	71
	Pd ²⁺	337.9	343.1	29
0.2%Pd-1.2%Ni/SBA-15	Pd ⁰	335.5	341.0	90
	Pd ²⁺	338.0	343.0	10
0.2%Pd-1.2%Ni/SBA-15 used	Pd ⁰	335.4	340.9	79
	Pd ²⁺	337.9	342.9	21

**Figure 6.** Relationship of the amount of surface Pd⁰ with the Ni loading amount.

Furthermore, Ni2p spectra were also analyzed for all 0.2%Pd-x%Ni/SBA-15 catalysts in Figure 5B (b–d). The observed Ni2p_{3/2} and Ni2p_{1/2} with the binding energies of 852.5 and 869.4 eV were ascribed to metallic Ni, and the Ni2p_{3/2} and Ni2p_{1/2} with the binding energies of 856.0 and 872.7 eV were ascribed to the oxidized state of Ni. It could be seen that most of the Ni is the nickel (II) species, and the fractions of the nickel (II) species in all 0.2%Pd-x%Ni/SBA-15 catalysts were approximately 90%, and only a small fraction of Ni was nickel (0) for all samples regardless of the Ni loading amount. The presence of nickel oxide also indicated that there was an electron transfer between Pd and Ni; at the same time, the sample exposed to air would also lead to the formation of nickel oxide [47–50].

2.4. Catalytic Performance

2.4.1. Hydrogenation of CAL to HALD over Pd-Ni/SBA-15

The catalytic performances were tested over the 0.2%Pd-x%Ni/SBA-15 catalysts. As listed in Table 3, the 1.2%Ni/SBA-15 catalyst only provided 29.0% conversion of CAL and 13.9% selectivity to HALD, indicating that 1.2%Ni/SBA-15 showed negligible catalytic performance in the process of selective hydrogenation. In addition, monometallic Pd supported on SBA-15 (0.2%Pd/SBA-15) showed 49.5% conversion of CAL and 48.0% selectivity to HALD. For 0.2%Pd-0.4%Ni/SBA-15, it performed 60.6% CAL conversion and 66.4% selectivity to HALD, and the selectivity to hydrocinnamal alcohol (HALC), COL and other by-products were 10.6%, 0.8%, and 22.2%, respectively. When the loading amount of Ni increased to 0.7 wt %, the conversion of CAL increased to 90.9% and the selectivity to HALD reached 83.2% over 0.2%Pd-0.7%Ni/SBA-15. Interestingly, the 0.2%Pd-1.2%Ni/SBA-15 catalyst showed 96.3% conversion of CAL and 87.8% selectivity to HALD, and the selectivity to other side products decreased to 0.3%. In addition, the hydrogenation of CAL is a complicated process, and often

yields many by-products. According to the literature [51–55], the other products possibly include 1-phenylpropane [51–54], β -methyl styrene [51–54], cinnamic acid [54,55], cinnamyl formate [54,55], benzyl cinnamate [54,55], 1-(3-propoxyprop-1-enyl)benzene [55], 4,4-diphenylcyclohexa-1,5-dienyl acetate [55], and other condensation products that could not be identified by gas chromatography-mass spectrometer (GC-MS) due to their large molecular weights [55]. Moreover, very little COL was observed for the 0.2%Pd/SBA-15 and 0.2%Pd-x%Ni/SBA-15 catalysts, similar to what has been previously reported on Pd catalysts [56,57].

Table 3. Selective hydrogenation activity of CAL over 0.2%Pd-x%Ni/SBA-15 ^a.

Sample	Conversion (%)	Selectivity (%)			
		HALD	HALC	COL	Others
1.2%Ni/SBA-15	29.0	13.9	12.1	0.6	73.4
0.2%Pd/SBA-15	49.5	48.0	7.4	1.4	42.7
0.2%Pd-0.4%Ni/SBA-15	60.6	66.4	10.6	0.8	22.2
0.2%Pd-0.7%Ni/SBA-15	90.9	83.2	10.9	0.1	5.8
0.2%Pd-1.2%Ni/SBA-15	96.3	87.8	11.7	0.2	0.3

^a Reaction conditions: 12.5 mg catalyst, 250 mg CAL, 15 mL isopropanol, 12 bar H₂, 2 h, 80 °C.

Therefore, it is obvious that the introduction of Ni can evidently enhance the catalytic performance of Pd on SBA-15 for CAL conversion and HALD selectivity. Of all the 0.2%Pd-x%Ni/SBA-15 catalysts, the 0.2%Pd-1.2%Ni/SBA-15 catalyst showed the best performance. In other words, the bimetallic catalyst is formed by a small proportion of Pd with the addition of Ni that exhibits a much higher hydrogenation performance than the monometallic Pd catalyst with the same Pd loading amount. The enhancement of activity can be ascribed to the synergistic effect between the Pd and Ni particles, which changes the electronic structure of the surface Pd species as examined by XPS. Through investigating the relationship between the yield of HALD and the amount of surface Pd⁰ over the 0.2%Pd/SBA-15 and 0.2%Pd-x%Ni/SBA-15 catalysts, it can be safely concluded that the yield of HALD increased along with the increased content of Pd⁰. Therefore, it indicates that both the high conversion of CAL and excellent selectivity to HALD over the 0.2%Pd-x%Ni/SBA-15 catalysts were caused by the high amount of the surface Pd⁰. This is in keeping with our previous studies where a large number of surface Pd⁰ species enhanced the hydrogenation activity of the substrates [7,9,58].

Table S2 summarizes the selective hydrogenation of CAL over the Pd-based catalysts reported from the literature. The 5.0 wt %Pd/MWCNT catalyst designed by Zhao et al. gave 91.3% HALD selectivity at 98.6% CAL conversion under 40 bar H₂ pressure and 148 bar CO₂ pressure [59]. Chen et al. reported 80% HALD selectivity with 100% CAL conversion over 3.0 wt % Pd/(SH)MSC catalyst [3]. 100% conversion of CAL and 97% HALD selectivity were obtained by using 0.7 wt %Pd/ γ -Al₂O₃ under 20 bar H₂ pressure in 3 h at 100 °C [60]. Wang et al. reported 86% HALD selectivity and almost 100% CAL conversion over the Pd catalyst supported on La₂O₂CO₃ nanorods [23]. Yang et al. used Pd supported on a silica modified titanate nanotube catalyst to obtain 84% HALD selectivity and 80% CAL conversion at 30 °C in 150 min [61]. When the reaction was carried out over the 1.5%Pd-MWCNT/AC catalyst, 41.8% conversion of CAL and 95.9% selectivity to HALD were gained by Ribeiro et al. [62]. Zhao et al. reported higher than 99.9% conversion of CAL with 90.4% HALD selectivity by using a 1.0 wt %Pd/ZIF-8 catalyst under 20 bar H₂ pressure in 6 h at 40 °C [63]. In summary, the bimetallic 0.2%Pd-1.2%Ni/SBA-15 catalyst still showed excellent catalytic performance with a low usage of Pd when compared with the above reported Pd-based catalysts in the literature.

2.4.2. Effect of H₂ Pressure over 0.2%Pd-1.2%Ni/SBA-15

The influence of hydrogen pressure on the hydrogenation of CAL to HALD over the 0.2%Pd-1.2%Ni/SBA-15 catalyst was investigated by varying the hydrogen pressure in the scope

of 8–16 bar. As given in Table 4, the hydrogen pressure could affect the CAL conversion and HALD selectivity to some extent. When the hydrogen pressure was 8 bar, 86.3% conversion of CAL and 71.2% selectivity to HALD were obtained. When the H₂ pressure was increased from 8 bar to 10 bar, the conversion of CAL as well as the selectivity to HALD improved to 87.3% and 80.7%, respectively. Upon increasing the hydrogen pressure to 12 bar, the conversion of CAL increased to 96.3% and the selectivity of HALD increased to 87.8%, which might be due to the fact that high pressure can enhance hydrogen solubility in an isopropanol solvent, thus leading to more hydrogen molecules close to the reaction medium [30]. With further increases in hydrogen pressure, the conversion of CAL increased to nearly 100%, whereas the HALD selectivity was slightly decreased, and the production of completely hydrogenated HALC was favorable, indicating the enhancement of the activity for the C=O bond along with the increase of the hydrogen pressure. Thus, the preferred hydrogen pressure was 12 bar in the present work.

Table 4. Effect of H₂ pressure on activity over 0.2%Pd-1.2%Ni/SBA-15 ^a.

H ₂ Pressure (bar)	Conversion (%)	Selectivity (%)			
		HALD	HALC	COL	Others
8	86.3	71.2	9.4	0.4	19.0
10	87.3	80.7	9.5	0.1	9.7
12	96.3	87.8	11.7	0.2	0.3
14	98.1	79.7	12.6	0.1	7.6
16	99.8	76.7	14.4	0	8.9

^a Reaction conditions: 12.5 mg catalyst, 250 mg CAL, 15 mL isopropanol, 2 h, 80 °C.

2.4.3. Effect of Reaction Temperature over 0.2%Pd-1.2%Ni/SBA-15

The influence of reaction temperature on the conversion and the selectivity to different products was investigated by varying the reaction temperature in the 40–100 °C range over 0.2%Pd-1.2%Ni/SBA-15. As shown in Table 5, the increase of the hydrogenation temperature favored the conversion of CAL, which increased from 30.1% (40 °C) to 99.5% (100 °C). In addition, the selectivity of HALD also increased significantly from 52.8% to 87.8% with the temperature from 40 °C to 80 °C, but decreased to 84.3% at 100 °C. This is explained by the fact that the hydrogenation of HALD to HALC was improved at a higher reaction temperature, thus leading to the complete hydrogenation of CAL to yield HALC as the final product.

Table 5. Effect of reaction temperature on activity over 0.2%Pd-1.2%Ni/SBA-15 ^a.

Temperature (°C)	Conversion (%)	Selectivity (%)			
		HALD	HALC	COL	Others
40	30.1	52.8	9.9	1.6	35.7
60	52.6	74.5	10.9	0.8	13.8
80	96.3	87.8	11.7	0.2	0.3
100	99.5	84.3	15.0	0.1	0.6

^a Reaction conditions: 12.5 mg catalyst, 250 mg CAL, 15 mL isopropanol, 12 bar H₂, 2 h.

2.4.4. Effect of Reaction Time over 0.2%Pd-1.2%Ni/SBA-15

The catalysis characteristic of 0.2%Pd-1.2%Ni/SBA-15 for the CAL hydrogenation was further explored by changing the reaction time, and the result is presented in Table 6. Obviously, the CAL conversion increased with a prolonged reaction time and attained 100% for 3 h, but the selectivity to HALD decreased slightly. This implies that the C=O group of HALD was difficult to activate under

the above reaction conditions. Otherwise, one would expect the selectivity to HALD to diminish with time because of the reduction in the amount of HALD as a result of its hydrogenation to HALC [24,64].

Table 6. Effect of reaction time on activity over 0.2%Pd-1.2%Ni/SBA-15 ^a.

Time (h)	Conversion (%)	Selectivity (%)			
		HALD	HALC	COL	Others
0.5	71.8	87.3	11.7	0.1	0.9
1	79.7	86.3	11.5	0.1	2.1
2	96.3	87.8	11.7	0.2	0.3
3	100	85.6	11.9	0.4	2.1

^a Reaction conditions: 12.5 mg catalyst, 250 mg CAL, 15 mL isopropanol, 12 bar H₂, 80 °C.

2.4.5. Activity Stability of 0.2%Pd-1.2%Ni/SBA-15

It should be noted that the stability of the catalysts in the hydrogenation of CAL to HALD is very important. Thus, the reusability of 0.2%Pd-1.2%Ni/SBA-15 was further studied (Figure 7). The used catalyst was separated by centrifugation with isopropanol several times after each test. It was observed that the CAL conversion and HALD selectivity decreased to 80.1% and 75.7% after two cycles of the catalyst, respectively. After the third cycle, the conversion and selectivity decreased to 65.7% and 66.4%, respectively. It was noteworthy that the catalyst remained stable up to fourth uses, both the conversion of CAL and the selectivity to HALD were maintained at about 60.0%. In order to find the reasons for deactivation, the 0.2%Pd-1.2%Ni/SBA-15 catalyst after two runs was characterized by XRF (Table 1), low-angle XRD (Figure S4), wide-angle XRD (Figure S5), N₂ adsorption-desorption measurements (Table 1), and XPS (Figure S6). The XRF analysis indicated that the Pd and Ni contents of the 0.2%Pd-1.2%Ni/SBA-15-used catalyst were about 0.17 wt % and 1.20 wt %, respectively, which suggested that there was trace leaching of Pd and Ni during the catalytic reactions. Therefore, the slight loss of metals was not the reason for the catalyst deactivation. In addition, when compared with the fresh 0.2%Pd-1.2%Ni/SBA-15 sample, the results of the low-angle XRD, wide-angle XRD as well as the N₂ adsorption-desorption of the reused catalyst were almost unchanged after twice recycling. However, a significant change of the surface Pd species was observed for the used catalyst. As shown in Table 2, the fraction of the Pd⁰ species decreased from 90% to 79%. The larger Pd²⁺ content on the catalyst surface contributed to the formation of side products with high-molecular weights. In other words, the deactivation reason can be ascribed to the reduction of the Pd⁰ amount on the surface of the 0.2%Pd-1.2%Ni/SBA-15 catalyst [58,61]. In addition, the used catalyst was reduced with hydrogen, and the activity for CAL hydrogenation was measured. The results showed that the CAL conversion and the HALD selectivity reached 85.1% and 84.0% over the reduced used catalyst, respectively. Therefore, the catalyst could partially restore its catalytic activity through reduction.

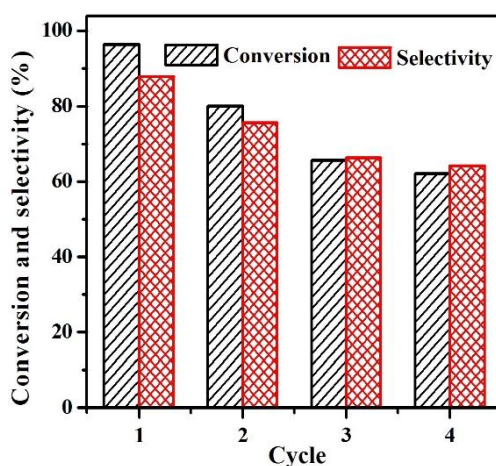


Figure 7. Stability test for 0.2%Pd-1.2%Ni/SBA-15 (Reaction conditions: 12.5 mg catalyst, 250 mg CAL, 15 mL isopropanol, 80 °C, 2 h, 12 bar H₂).

3. Experimental Sections

3.1. Chemicals

Tetraethyl orthosilicate (TEOS) and PdCl₂ were purchased from the Tianjin Kermel Chemical Reagent Co., Ltd., Tianjin, China; Ni(NO₃)₂·6H₂O was purchased from the Tianjin Fortune Chemical Reagent Co., Ltd., Tianjin, China; and Triblock poly(ethylene oxide)-b-poly(propylene oxide)-b-poly(ethylene oxide) copolymer Pluronic P123 (M_w = 5800, EO₂₀PO₇₀EO₂₀) was purchased from Aldrich. CAL was purchased from Aladdin. Isopropanol was purchased from the Tianjin Fuyu Fine Chemical Co., Ltd., Tianjin, China.

3.2. Catalyst Preparation

The preparation of pure silica SBA-15 was performed following the reported literature [65]. The 0.2%Pd-*x*%Ni/SBA-15 (*x* = 0.4, 0.7, and 1.2) catalysts were synthesized through impregnation combined with the NaBH₄ reduction method. Typically, 0.300 g of SBA-15 silica support was impregnated with 10 mL deionized H₂O with a certain amount of PdCl₂ solution (Pd content of 6.0 mg/g) and Ni(NO₃)₂·6H₂O precursor poured into the solution, and the suspension was stirred for 12 h. Afterwards, the pH of the solution was adjusted to 10.0 using a NaOH solution (1 mol/L). Then, the mixture was placed in an ice bath with vigorous stirring for 0.5 h, and the temperature was maintained at 2–4 °C. Subsequently, the excessive NaBH₄ was added dropwise to the above mixture, which was vigorously stirred for about 4 h to reduce the high oxidation state of the metals. Finally, the 0.2%Pd-*x*%Ni/SBA-15 catalysts were obtained by filtration with a large amount of deionized water and ethanol in sequence and dried at 60 °C for 10 h in a vacuum oven. For comparison, the 0.2%Pd/SBA-15 and 1.2%Ni/SBA-15 catalysts were also prepared under similar conditions.

3.3. Catalyst Characterizations

Wide-angle X-ray diffraction (XRD) patterns were performed on Rigaku D/max-III B diffractometer equipment (Rigaku Industrial Corporation, Tokyo, Japan) with Cu Kα (λ = 1.5418 Å) radiation (40 kV, 20 mA) in the range of 10–80°. For the low-angle XRD patterns, the scan scope was 0.5–5°, and the scanning rate was 1°/min. N₂ adsorption-desorption isotherms were measured with a Micromeritics Tristar II (Micromeritics Instrument Corporation, Norcross, USA) at −196 °C, and the Brunauer-Emmett-Teller (BET) specific surface areas were calculated from the adsorption data. The pore size distributions were determined from the adsorption branches of the isotherms by using the (BJH) method. X-ray photoelectron spectroscopy (XPS) measurements were carried out by

using a Kratos-AXIS ULTRA DLD (Kratos Analytical Limited, Kyoto, Japan) with a monochromatic Al K α radiation source. Transmission electron microscopy (TEM) experiments were analyzed using a JOEL model JEM-210 (JEOL, Tokyo, Japan) electron microscope with an acceleration voltage of 200 kV. X-ray fluorescence spectrometry (XRF) was used to analyze the metals content by using a Bruker S4 Explorer instrument (Bruker Corporation, Billerica, MA, USA).

3.4. Hydrogenation of CAL

The hydrogenation reaction of CAL was performed in a 100 mL autoclave. Typically, CAL (0.25 g), catalyst (12.5 mg) and isopropanol (15 mL) were introduced into an autoclave fitted with a emperature-controlled furnace. Afterwards, the reactor was introduced three times with N₂ and three times with H₂ to remove the air. Subsequently, the reactor was filled with the specific hydrogen pressure (8–16 bar) and heated to the required temperature (40–100 °C) under magnetic stirring for 0.5–3 h. After the reaction, the solution was filtered to screen out the catalyst, and the products were detected by gas chromatography (BFRL SP-3420, Beijing, Chain) equipped with flame ionization detection (FID) as well as a HP-5 capillary column (30 m \times 0.32 mm \times 0.25 μ m) using octanol as the external standard. Therefore, the conversion of CAL and the selectivity to different products were calculated by using Equations (1)–(5).

$$\text{Conversion of CAL} = (n_0 - n_{(\text{CAL})})/n_0 \times 100\% \quad (1)$$

$$\text{Selectivity of HALD} (S_{\text{HALD}}) = n_{(\text{HALD})}/(n_0 - n_{(\text{CAL})}) \times 100\% \quad (2)$$

$$\text{Selectivity of HALC} (S_{\text{HALC}}) = n_{(\text{HALC})}/(n_0 - n_{(\text{CAL})}) \times 100\% \quad (3)$$

$$\text{Selectivity of COL} (S_{\text{COL}}) = n_{(\text{COL})}/(n_0 - n_{(\text{CAL})}) \times 100\% \quad (4)$$

$$\text{Selectivity of side products} (S_{\text{others}}) = (100\% - S_{\text{HALD}} - S_{\text{HALC}} - S_{\text{COL}}) \quad (5)$$

where n_0 and $n_{(\text{CAL})}$ represent the molar amount of the original CAL and residual CAL after reaction and $n_{(\text{HALD})}$, $n_{(\text{HALC})}$, and $n_{(\text{COL})}$ are the molar content of the formed HALD, HALC and COL, respectively.

4. Conclusions

A series of catalysts (0.2%Pd- x %Ni/SBA-15, $x = 0.4, 0.7$ and 1.2) were prepared and evaluated for the liquid-phase hydrogenation of CAL. Typically, the introduction of Ni to 0.2%Pd/SBA-15 could evidently improve the catalytic performance of Pd as a result of the strong interaction between Pd and Ni. Of all the catalysts, 0.2%Pd-1.2%Ni/SBA-15 showed the best performance with 96.3% conversion and 87.8% selectivity toward the HALD. This illustrated that Ni could be a co-catalyst of Pd, promoting its catalytic performance in the selective hydrogenation of CAL. This improvement can be attributed to the synergistic effect between Pd and Ni where first, the addition of Ni favors the dispersion of the Pd nanoparticles; and second, the Ni increases the amount of surface Pd⁰ on the catalysts.

Supplementary Materials: The following are available online at <http://www.mdpi.com/2073-4344/8/5/200/s1>, Table S1: Selective hydrogenation of cinnamaldehyde to hydrocinnamaldehyde over heterogeneous catalysts from the literature, Table S2: Details of the hydrogenation of CAL to HALD using Pd based catalysts, Figure S1: The pore size distributions calculated from the desorption using the BJH method for (a) SBA-15, (b) 0.2%Pd/SBA-15, (c) 0.2%Pd-0.4%Ni/SBA-15, (d) 0.2%Pd-0.7%Ni/SBA-15, (e) 0.2%Pd-1.2%Ni/SBA-15, Figure S2: Wide-angle XRD patterns of (a) 0.9%Pd/SBA-15, (b) 0.9%Pd-0.4%Ni/SBA-15, (c) 0.9%Pd-0.7%Ni/SBA-15, (d) 0.9%Pd-1.2%Ni/SBA-15, Figure S3: TEM images of (a–b) 0.9%Pd/SBA-15, (c–d) 0.9%Pd-1.2%Ni/SBA-15, Figure S4: Low-angle XRD patterns for the fresh and reused 0.2%Pd-1.2%Ni/SBA-15 catalyst, Figure S5: Wide-angle XRD patterns for the fresh and reused 0.2%Pd-1.2%Ni/SBA-15 catalyst, Figure S6: Pd3d XPS spectra for the fresh and reused 0.2%Pd-1.2%Ni/SBA-15 catalyst.

Author Contributions: Y.Z. proposed, planned, and designed the experiments. S.H. performed the experimental works. S.H., Y.L., J.L., R.L., and F.Y. contributed to the data analysis. S.H. and Y.Z. wrote the manuscript. Y.Z. supervised the project. All authors discussed the results and approved the manuscript.

Acknowledgments: This work was supported by the Natural Sciences Fund of Heilongjiang Province (B2015009) and the Innovative Research Project of Key Laboratory of Functional Inorganic Material Chemistry (Heilongjiang University), Ministry of Education (2015).

Conflicts of Interest: The authors declare no conflict of interest.

References

1. Hong, Y.C.; Sun, K.Q.; Zhang, G.R.; Zhong, R.Y.; Xu, B.Q. Fully dispersed Pt entities on nano-Au dramatically enhance the activity of gold for chemoselective hydrogenation catalysis. *Chem. Commun.* **2011**, *47*, 1300–1302. [[CrossRef](#)] [[PubMed](#)]
2. Yepez, A.; Hidalgo, J.M.; Pineda, A.; Černý, R.; Jiša, P.; Garcia, A.; Romero, A.A.; Luque, R. Mechanistic insights into the hydroconversion of cinnamaldehyde using mechanochemically synthesized Pd/Al-SBA-15 catalysts. *Green Chem.* **2015**, *17*, 565–572. [[CrossRef](#)]
3. Chen, S.J.; Meng, L.; Chen, B.X.; Chen, W.Y.; Duan, X.Z.; Huang, X.; Zhang, B.S.; Fu, H.B.; Wan, Y. Poison Tolerance to the Selective Hydrogenation of Cinnamaldehyde in Water over an Ordered Mesoporous Carbonaceous Composite Supported Pd Catalyst. *ACS Catal.* **2017**, *7*, 2074–2087. [[CrossRef](#)]
4. Reddy, B.M.; Kumar, G.M.; Ganesh, I.; Khan, A. Vapour phase hydrogenation of cinnamaldehyde over silica supported transition metal-based bimetallic catalysts. *J. Mol. Catal. A Chem.* **2006**, *247*, 80–87. [[CrossRef](#)]
5. Lin, W.W.; Cheng, H.Y.; He, L.M.; Yu, Y.C.; Zhao, F.Y. High performance of Ir-promoted Ni/TiO₂ catalyst toward the selective hydrogenation of cinnamaldehyde. *J. Catal.* **2013**, *303*, 110–116. [[CrossRef](#)]
6. Ji, X.W.; Niu, X.Y.; Li, B.; Han, Q.; Yuan, F.L.; Zaera, F.; Zhu, Y.J.; Fu, H.G. Selective Hydrogenation of Cinnamaldehyde to Cinnamal Alcohol over Platinum/Graphene Catalysts. *ChemCatChem* **2014**, *6*, 3246–3253. [[CrossRef](#)]
7. Han, Q.; Liu, Y.F.; Wang, D.; Yuan, F.L.; Niu, X.Y.; Zhu, Y.J. Effect of carbon nanosheets with different graphitization degrees as a support of noble metals on selective hydrogenation of cinnamaldehyde. *RSC Adv.* **2016**, *6*, 98356–98364. [[CrossRef](#)]
8. Wang, D.; Zhu, Y.J.; Tian, C.G.; Wang, L.; Zhou, W.; Dong, Y.L.; Han, Q.; Liu, Y.F.; Yuan, F.L.; Fu, H.G. Synergistic effect of Mo₂N and Pt for promoted selective hydrogenation of cinnamaldehyde over Pt–Mo₂N/SBA-15. *Catal. Sci. Technol.* **2016**, *6*, 2403–2412. [[CrossRef](#)]
9. Wang, D.; Zhu, Y.J.; Tian, C.G.; Wang, L.; Zhou, W.; Dong, Y.L.; Yan, H.J.; Fu, H.G. Synergistic Effect of Tungsten Nitride and Palladium for the Selective Hydrogenation of Cinnamaldehyde at the C=C bond. *ChemCatChem* **2016**, *8*, 1718–1726. [[CrossRef](#)]
10. Zheng, Q.; Wang, D.; Yuan, F.L.; Han, Q.; Dong, Y.L.; Liu, Y.F.; Niu, X.Y.; Zhu, Y.J. An Effective Co-promoted Platinum of Co–Pt/SBA-15 Catalyst for Selective Hydrogenation of Cinnamaldehyde to Cinnamyl Alcohol. *Catal. Lett.* **2016**, *146*, 1535–1543. [[CrossRef](#)]
11. Bhogswararao, S.; Srinivas, D. Intramolecular selective hydrogenation of cinnamaldehyde over CeO₂–ZrO₂-supported Pt catalysts. *J. Catal.* **2012**, *285*, 31–40. [[CrossRef](#)]
12. Wei, S.P.; Zhao, Y.T.; Fan, G.L.; Yang, L.; Li, F. Structure-dependent selective hydrogenation of cinnamaldehyde over high-surface-area CeO₂–ZrO₂ composites supported Pt nanoparticles. *Chem. Eng. J.* **2017**, *322*, 234–245. [[CrossRef](#)]
13. Kahsar, K.R.; Schwartz, D.K.; Medlin, J.W. Stability of self-assembled monolayer coated Pt/Al₂O₃ catalysts for liquid phase hydrogenation. *J. Mol. Catal. A Chem.* **2015**, *396*, 188–195. [[CrossRef](#)]
14. Vriamont, C.; Haynes, T.; McCague-Murphy, E.; Pannetreau, F.; Riant, O.; Hermans, S. Covalently and non-covalently immobilized clusters onto nanocarbons as catalysts precursors for cinnamaldehyde selective hydrogenation. *J. Catal.* **2015**, *329*, 389–400. [[CrossRef](#)]
15. Ide, M.S.; Hao, B.; Neurock, M.; Davis, R.J. Mechanistic Insights on the Hydrogenation of α,β -Unsaturated Ketones and Aldehydes to Unsaturated Alcohols over Metal Catalysts. *ACS Catal.* **2012**, *2*, 671–683. [[CrossRef](#)]
16. Chen, H.N.; Cullen, D.A.; Larese, J.Z. Highly Efficient Selective Hydrogenation of Cinnamaldehyde to Cinnamyl Alcohol over Gold Supported on Zinc Oxide Materials. *J. Phys. Chem. C* **2015**, *119*, 28885–28894. [[CrossRef](#)]

17. Machado, B.F.; Gomes, H.T.; Serp, P.; Kalck, P.; Faria, J.L. Liquid-Phase Hydrogenation of Unsaturated Aldehydes: Enhancing Selectivity of Multiwalled Carbon Nanotube-Supported Catalysts by Thermal Activation. *ChemCatChem* **2010**, *2*, 190–197. [[CrossRef](#)]
18. Reyes, P.; Rojas, H.; Fierro, J.L.G. Kinetic study of liquid-phase hydrogenation of citral over Ir/TiO₂ catalysts. *Appl. Catal. A* **2003**, *248*, 59–65. [[CrossRef](#)]
19. Li, Y.; Li, Z.G.; Zhou, R.X. Bimetallic Pt-Co catalysis on carbon nanotubes for the selective hydrogenation of cinnamaldehyde to cinnamyl alcohol: Preparation and characterization. *J. Mol. Catal. A Chem.* **2008**, *279*, 140–146. [[CrossRef](#)]
20. Tsang, S.C.; Cailuo, N.; Oduro, W.; Kong, A.T.S.; Clifton, L.; Yu, K.M.K.; Thiebaut, B.; Cookson, J.; Bishop, P. Engineering Preformed Cobalt-Doped Platinum Nanocatalysts for Ultrasensitive Hydrogenation. *ACS Nano* **2008**, *2*, 2547–2553. [[CrossRef](#)] [[PubMed](#)]
21. Gutiérrez, V.S.; Diez, A.S.; Dennehy, M.; Volpe, M.A. Cu incorporated MCM-48 for the liquid phase hydrogenation of cinnamaldehyde. *Microporous Mesoporous Mater.* **2011**, *141*, 207–213. [[CrossRef](#)]
22. Siddiqui, N.; Sarkar, B.; Pendem, C.; Khatun, R.; Konthala, L.N.S.; Sasaki, T.; Bordoloia, A.; Bal, R. Highly selective transfer hydrogenation of α,β -unsaturated carbonyl compounds using Cu-based nanocatalysts. *Catal. Sci. Technol.* **2017**, *7*, 2828–2837. [[CrossRef](#)]
23. Wang, F.; Zhang, Z.N.; Wei, X.J.; Fang, Q.H.; Jiang, X.M. The shape effect of La₂O₂CO₃ in Pd/La₂O₂CO₃ catalyst for selective hydrogenation of cinnamaldehyde. *Appl. Catal. A* **2017**, *543*, 196–200. [[CrossRef](#)]
24. Nagpure, A.S.; Gurralla, L.; Gogoi, P.; Chilukuri, S.V. Hydrogenation of cinnamaldehyde to hydrocinnamaldehyde over Pd nanoparticles deposited on nitrogen-doped mesoporous carbon. *RSC Adv.* **2016**, *6*, 44333–44340. [[CrossRef](#)]
25. Vicente, A.; Ekou, T.; Lafaye, G.; Especel, C.; Marécot, P.; Williams, C.T. Influence of the nature of the precursor salts on the properties of Rh–Ge/TiO₂ catalysts for citral hydrogenation. *J. Catal.* **2010**, *275*, 202–210. [[CrossRef](#)]
26. Reyes, P.; Aguirre, M.C.; Fierro, J.L.G.; Santori, G.; Ferretti, O. Hydrogenation of crotonaldehyde on Rh-Sn/SiO₂ catalysts prepared by reaction of tetrabutyltin on prereduced Rh/SiO₂ precursors. *J. Mol. Catal. A Chem.* **2002**, *184*, 431–441. [[CrossRef](#)]
27. Prakash, M.G.; Mahalakshmy, R.; Krishnamurthy, K.R.; Viswanathan, B. Selective hydrogenation of cinnamaldehyde on nickel nanoparticles supported on titania: Role of catalyst preparation methods. *Catal. Sci. Technol.* **2015**, *5*, 3313–3321. [[CrossRef](#)]
28. Zaramello, L.; Albuquerque, B.L.; Domingos, J.B.; Philippot, K. Kinetic investigation into the chemoselective hydrogenation of α,β -unsaturated carbonyl compounds catalyzed by Ni(0) nanoparticles. *Dalton Trans.* **2017**, *46*, 5082–5090. [[CrossRef](#)] [[PubMed](#)]
29. Gryglewicz, S.; Sliwak, A.; Cwikła, J.; Gryglewicz, G. Performance of Carbon Nanofiber and Activated Carbon Supported Nickel Catalysts for Liquid-Phase Hydrogenation of Cinnamaldehyde into Hydrocinnamaldehyde. *Catal. Lett.* **2014**, *144*, 62–69. [[CrossRef](#)]
30. Yang, X.; Chen, D.; Liao, S.J.; Song, H.Y.; Li, Y.W.; Fu, Z.Y.; Su, Y.L. High-performance Pd–Au bimetallic catalyst with mesoporous silica nanoparticles as support and its catalysis of cinnamaldehyde hydrogenation. *J. Catal.* **2012**, *291*, 36–43. [[CrossRef](#)]
31. Zheng, R.Y.; Porosoff, M.D.; Weiner, J.L.; Lu, S.L.; Zhu, Y.X.; Chen, J.G. Controlling hydrogenation of C=O and C=C bonds in cinnamaldehyde using silica supported Co-Pt and Cu-Pt bimetallic catalysts. *Appl. Catal. A* **2012**, *419–420*, 126–132. [[CrossRef](#)]
32. Sun, K.Q.; Hong, Y.C.; Zhang, G.R.; Xu, B.Q. Synergy between Pt and Au in Pt-on-Au Nanostructures for Chemoselective Hydrogenation Catalysis. *ACS Catal.* **2011**, *1*, 1336–1346. [[CrossRef](#)]
33. Wu, S.H.; Mou, C.Y.; Lin, H.P. Synthesis of mesoporous silica nanoparticles. *Chem. Soc. Rev.* **2013**, *42*, 3862–3875. [[CrossRef](#)] [[PubMed](#)]
34. Gutiérrez, L.F.; Hamoudi, S.; Belkacemi, K. Synthesis of Gold Catalysts Supported on Mesoporous Silica Materials: Recent Developments. *Catalysts* **2011**, *1*, 97–154. [[CrossRef](#)]
35. Kresge, C.T.; Leonowicz, M.E.; Roth, W.J.; Vartuli, J.C.; Beck, J.S. Ordered mesoporous molecular sieves synthesized by a liquid-crystal template mechanism. *Nature* **1992**, *359*, 710–712. [[CrossRef](#)]
36. Zhu, J.J.; Wang, T.; Xu, X.L.; Xiao, P.; Li, J.L. Pt nanoparticles supported on SBA-15: Synthesis, characterization and applications in heterogeneous catalysis. *Appl. Catal. B* **2013**, *130–131*, 197–217. [[CrossRef](#)]

37. Loricera, C.V.; Pawelec, B.; Infantes-Molina, A.; Álvarez-Galvana, M.C.; Huirache-Acuna, R.; Nava, R.; Fierro, J.L.G. Hydrogenolysis of anisole over mesoporous sulfided CoMoW/SBA-15(16) catalysts. *Catal. Today* **2011**, *172*, 103–110. [[CrossRef](#)]
38. Ungureanu, A.; Dragoi, B.; Chiriac, A.; Ciotonea, C.; Royer, S.; Duprez, D.; Mamede, A.S.; Dumitriu, E. Composition-Dependent morphostructural properties of Ni–Cu oxide nanoparticles confined within the channels of ordered mesoporous SBA-15 silica. *ACS Appl. Mater. Interfaces* **2013**, *5*, 3010–3025. [[CrossRef](#)] [[PubMed](#)]
39. Karthikeyan, S.; Pachamuthu, M.P.; Isaacs, M.A.; Kumar, S.; Lee, A.F.; Sekaran, G. Cu and Fe oxides dispersed on SBA-15: A Fenton type bimetallic catalyst for *N,N*-diethyl-*p*-phenyl diamine degradation. *Appl. Catal. B* **2016**, *199*, 323–330. [[CrossRef](#)]
40. Zhang, P.; Liu, C.H.; Chen, L.; Chen, J.M.; Guan, Y.J.; Wu, P. Factors influencing the activity of SiO₂ supported bimetal Pd–Ni catalyst for hydrogenation of α -angelica lactone: Oxidation state, particle size, and solvents. *J. Catal.* **2017**, *351*, 10–18. [[CrossRef](#)]
41. Tang, W.X.; Deng, Y.Z.; Chen, Y.F. Promoting effect of acid treatment on Pd–Ni/SBA-15 catalyst for complete oxidation of gaseous benzene. *Catal. Commun.* **2017**, *89*, 86–90. [[CrossRef](#)]
42. Zhang, H.L.; Wang, Y.C.; Wang, Y.; Cao, J.L.; Kang, P.; Tang, Q.J.; Ma, M.J. Highly Dispersed PdNPs/ α -Al₂O₃ Catalyst for the Selective Hydrogenation of Acetylene Prepared with Monodispersed Pd Nanoparticles. *Catalysts* **2017**, *7*, 128–137. [[CrossRef](#)]
43. Volokitin, Y.; Sinzig, J.; Jongh, L.J.; Schmid, G.; Vargaftik, M.N.; Moiseev, I.I. Quantum-size effects in the thermodynamic properties of metallic nanoparticles. *Nature* **1996**, *384*, 621–623. [[CrossRef](#)]
44. Fu, X.Y.; Wang, Y.; Wu, N.Z.; Gui, L.L.; Tang, Y.Q. Surface modification of small platinum nanoclusters with alkylamine and alkylthiol: An XPS study on the influence of organic ligands on the Pt 4f binding energies of small platinum nanoclusters. *J. Colloid Interface Sci.* **2001**, *243*, 326–330. [[CrossRef](#)]
45. Shukla, S.; Seal, S. Cluster size effect observed for gold nanoparticles synthesized by sol-gel technique as studied by X-Ray Photoelectron Spectroscopy. *Nanostruct. Mater.* **1999**, *11*, 1181–1193. [[CrossRef](#)]
46. Liu, C.L.; Nan, C.S.; Fan, G.L.; Yang, L.; Li, F. Facile synthesis and synergistically acting catalytic performance of supported bimetallic PdNi nanoparticle catalysts for selective hydrogenation of citral. *Mol. Catal.* **2017**, *436*, 237–247. [[CrossRef](#)]
47. Cao, N.; Yang, L.; Dai, H.M.; Liu, T.; Su, J.; Wu, X.J.; Luo, W.; Cheng, G.Z. Immobilization of ultrafine bimetallic Ni–Pt nanoparticles inside the pores of metal–organic frameworks as efficient catalysts for dehydrogenation of alkaline solution of hydrazine. *Inorg. Chem.* **2014**, *53*, 10122–10128. [[CrossRef](#)] [[PubMed](#)]
48. Xia, J.W.; Fu, Y.S.; He, G.Y.; Sun, X.Q.; Wang, X. Core-shell-like Ni–Pd nanoparticles supported on carbon black as a magnetically separable catalyst for green Suzuki–Miyaura coupling reactions. *Appl. Catal. B* **2017**, *200*, 39–46. [[CrossRef](#)]
49. Zhong, D.C.; Aranishi, K.; Singh, A.k.; Demircib, U.B.; Xu, Q. The synergistic effect of Rh–Ni catalysts on the highly-efficient dehydrogenation of aqueous hydrazine borane for chemical hydrogen storage. *Chem. Commun.* **2012**, *48*, 11945–11947. [[CrossRef](#)] [[PubMed](#)]
50. Chen, B.F.; Li, F.B.; Huang, Z.J.; Yuan, G.Q. Tuning catalytic selectivity of liquid-phase hydrogenation of furfural via synergistic effects of supported bimetallic catalysts. *Appl. Catal. A* **2015**, *500*, 23–29. [[CrossRef](#)]
51. Poltarzewski, Z.; Galvagno, S.; Pietropaolo, R.; Staiti, P. Hydrogenation of α,β -Unsaturated Aldehydes over Pt–Sn/Nylon. *J. Catal.* **1986**, *102*, 190–198. [[CrossRef](#)]
52. Bus, E.; Prins, R.; Bokhoven, J.A. Origin of the cluster-size effect in the hydrogenation of cinnamaldehyde over supported Au catalysts. *Catal. Commun.* **2007**, *8*, 1397–1402. [[CrossRef](#)]
53. Merlo, A.B.; Machado, B.F.; Vetere, V.; Faria, J.L.; Casella, M.L. PtSn/SiO₂ catalysts prepared by surface controlled reactions for the selective hydrogenation of cinnamaldehyde. *Appl. Catal. A* **2010**, *383*, 43–49. [[CrossRef](#)]
54. Shi, J.J.; Nie, R.F.; Chen, P.; Hou, Z.Y. Selective hydrogenation of cinnamaldehyde over reduced grapheme oxide supported Pt catalyst. *Catal. Commun.* **2013**, *41*, 101–105. [[CrossRef](#)]
55. Guo, Z.; Chen, Y.T.; Li, L.S.; Wang, X.M.; Haller, G.L.; Yang, Y.H. Carbon nanotube-supported Pt-based bimetallic catalysts prepared by a microwave-assisted polyol reduction method and their catalytic applications in the selective hydrogenation. *J. Catal.* **2010**, *276*, 314–326. [[CrossRef](#)]
56. Hammoudeh, A.; Mahmoud, S. Selective hydrogenation of cinnamaldehyde over Pd/SiO₂ catalysts: Selectivity promotion by alloyed Sn. *J. Mol. Catal. A Chem.* **2003**, *203*, 231–239. [[CrossRef](#)]

57. Cairns, G.R.; Cross, R.J.; Stirling, D. Hydrogenation of cinnamaldehyde using catalysts prepared from supported palladium phosphine complexes. *J. Catal.* **1997**, *166*, 89–97. [[CrossRef](#)]
58. Zhang, F.; Liu, Y.F.; Yuan, F.L.; Niu, X.Y.; Zhu, Y.J. Efficient production of the liquid fuel 2,5-Dimethylfuran from 5-Hydroxymethylfurfural in the Absence of Acid Additive over bimetallic PdAu supported on graphitized carbon. *Energy Fuels* **2017**, *31*, 6364–6373. [[CrossRef](#)]
59. Zhao, B.H.; Chen, J.G.; Liu, X.; Liu, Z.W.; Hao, Z.P.; Xiao, J.L.; Liu, Z.T. Selective Hydrogenation of Cinnamaldehyde over Pt and Pd Supported on Multiwalled Carbon Nanotubes in a CO₂-Expanded Alcoholic Medium. *Ind. Eng. Chem. Res.* **2012**, *51*, 11112–11121. [[CrossRef](#)]
60. Galletti, A.M.R.; Antonetti, C.; Venezia, A.M.; Giambastiani, G. An easy microwave-assisted process for the synthesis of nanostructured palladium catalysts and their use in the selective hydrogenation of cinnamaldehyde. *Appl. Catal. A* **2010**, *385*, 124–131. [[CrossRef](#)]
61. Yang, X.; Wu, L.P.; Du, L.; Long, L.Z.; Wang, T.J.; Ma, L.L.; Li, X.J.; Liao, S.J. High performance Pd catalyst using silica modified titanate nanotubes (STNT) as support and its catalysis toward hydrogenation of cinnamaldehyde at ambient temperature. *RSC Adv.* **2014**, *4*, 63062–63069. [[CrossRef](#)]
62. Ribeiro, P.H.Z.; Matsubara, E.Y.; Rosolen, M.; Donate, P.M.; Gunnella, R. Palladium decoration of hybrid carbon nanotubes/charcoal composite and its catalytic behavior in the hydrogenation of trans-cinnamaldehyde. *J. Mol. Catal. A Chem.* **2015**, *410*, 34–40. [[CrossRef](#)]
63. Zhao, Y.; Liu, M.M.; Fan, B.B.; Chen, Y.F.; Lv, W.M.; Lu, N.Y.; Li, R.F. Pd nanoparticles supported on ZIF-8 as an efficient heterogeneous catalyst for the selective hydrogenation of cinnamaldehyde. *Catal. Commun.* **2014**, *57*, 119–123. [[CrossRef](#)]
64. Zhao, F.Y.; Ikushima, Y.; Chatterjee, M.; Shiraia, M.; Arai, M. An effective and recyclable catalyst for hydrogenation of α,β -unsaturated aldehydes into saturated aldehydes in supercritical carbon dioxide. *Green Chem.* **2003**, *5*, 76–79. [[CrossRef](#)]
65. Zhao, D.Y.; Feng, J.L.; Huo, Q.S.; Melosh, N.; Fredrickson, G.H.; Chmelka, B.F.; Stucky, G.D. Triblock copolymer syntheses of mesoporous silica with periodic 50 to 300 angstrom pores. *Science* **1998**, *279*, 548–552. [[CrossRef](#)] [[PubMed](#)]



© 2018 by the authors. Licensee MDPI, Basel, Switzerland. This article is an open access article distributed under the terms and conditions of the Creative Commons Attribution (CC BY) license (<http://creativecommons.org/licenses/by/4.0/>).